

Supplementary Information for “*Prediction of two-dimensional nodal-line semimetal in a carbon nitride covalent network*”

Haiyuan Chen,^{ab} Shunhong Zhang,^{cb} Wei Jiang,^b Chunxiao Zhang,^b Heng Guo,^a Zheng

Liu,^{cd} Zhiming Wang,^a Feng Liu,^{*bd} and Xiaobin Niu^{*a}

^a Institute of Fundamental and Frontier Sciences and School of Materials and Energy, University of Electronic Science and Technology of China, Chengdu 610054, P. R. China

^b Department of Materials Science and Engineering, University of Utah, Salt Lake City, UT 84112, USA

^c Institute for Advanced Study, Tsinghua University, Beijing 100084, P. R. China

^d Collaborative Innovation Center of Quantum Matter, Beijing 100084, P. R. China

Corresponding author: xbniu@uestc.edu.cn, fliu@eng.utah.edu

This PDF file includes:

- Atomic configurations for C₃N, C₂N, and C₉N₄.
- Band structures for C₉N₄ calculated with HSE functional
- Buckling effect on the C₉N₄ band structure.
- Band structures for C₉N₄ with SOC.
- Details about molecular properties of C₉N₄.
- Total energy comparison and band structure for AB-stacking and AA-stacking C₉N₄.
- Details related to the C₉N₄ Stability.

- Atomic configurations for C_3N , C_2N , and C_9N_4 .

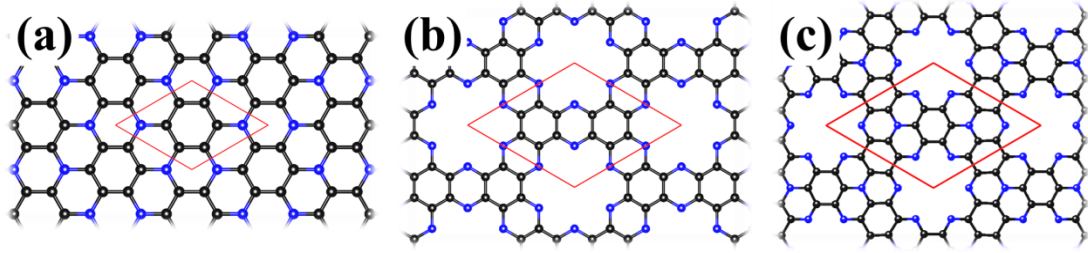


Fig. S1 Atomic configurations for (a) C_3N , (b) C_2N , and (c) C_9N_4 . The blue and black balls indicate nitrogen and carbon atoms. The unit cell is shown by red solid lines.

- Band structures for C_9N_4 calculated with HSE functional

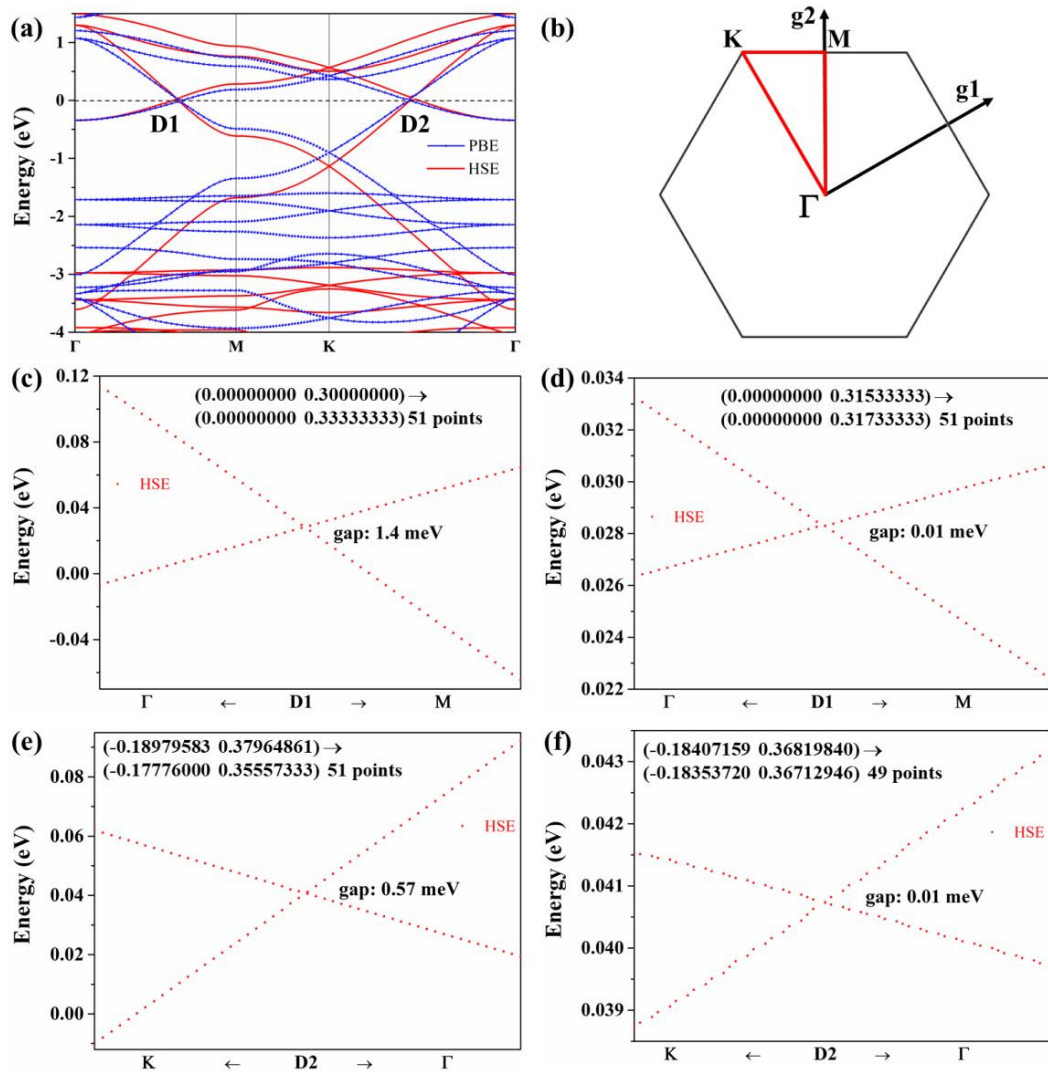


Fig. S2 (a) Comparison of band structure for 2D C_9N_4 with HSE and PBE functional. (b) BZ for 2D C_9N_4 . (c)-(d) Band structure close to D1 calculated with HSE functional. (e)-(f) Band structure close to D2 calculated with HSE functional. The fractional coordinates of two end points along smaller k-path and related total number of k-points are indicated in (c-f).

- Buckling effect on the C_9N_4 band structure.

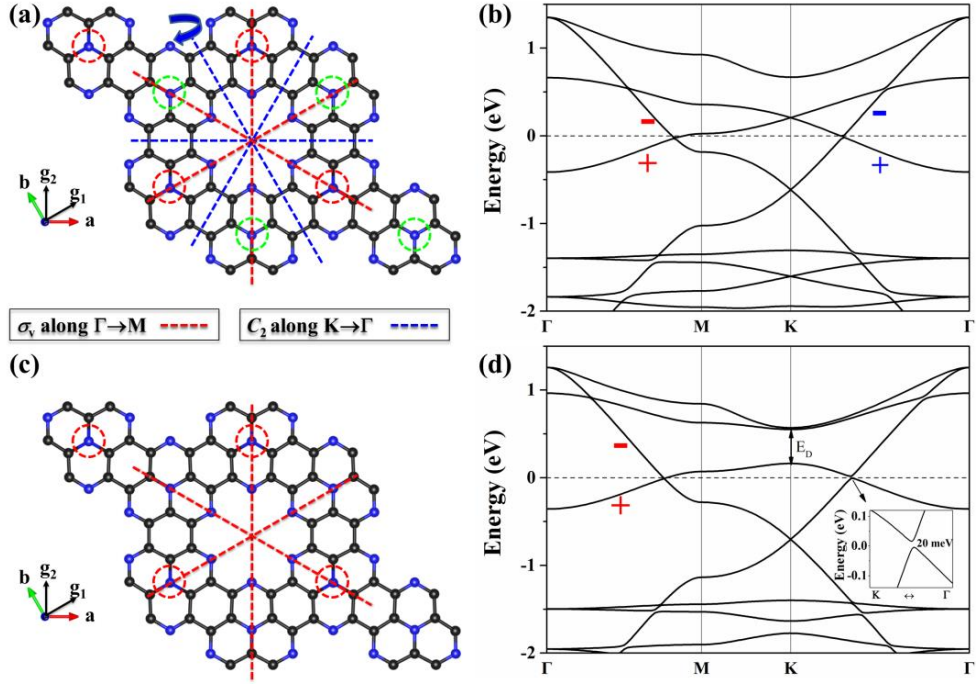


Fig. S3 (a) and (c) is the top view of two kinds of perturbations induced in C_9N_4 without in-plane mirror symmetry. The red and green circles indicate the atoms shifted upwards and downwards, respectively. The buckling height is 0.4 \AA for all structures. The red and blue dashed lines indicate the σ_v mirror plane and C_2 rotation axis, respectively. (b) and (d) is the band structure for (a) and (c), respectively. The “+” and “-” symbols indicate the parities of crossing bands with respect to σ_v mirror reflection and C_2 rotation along Γ -M and K- Γ respectively. The inset of (d) shows the opened gap of 20 meV along K to Γ near Fermi level.

- Band structures for C_9N_4 with SOC.

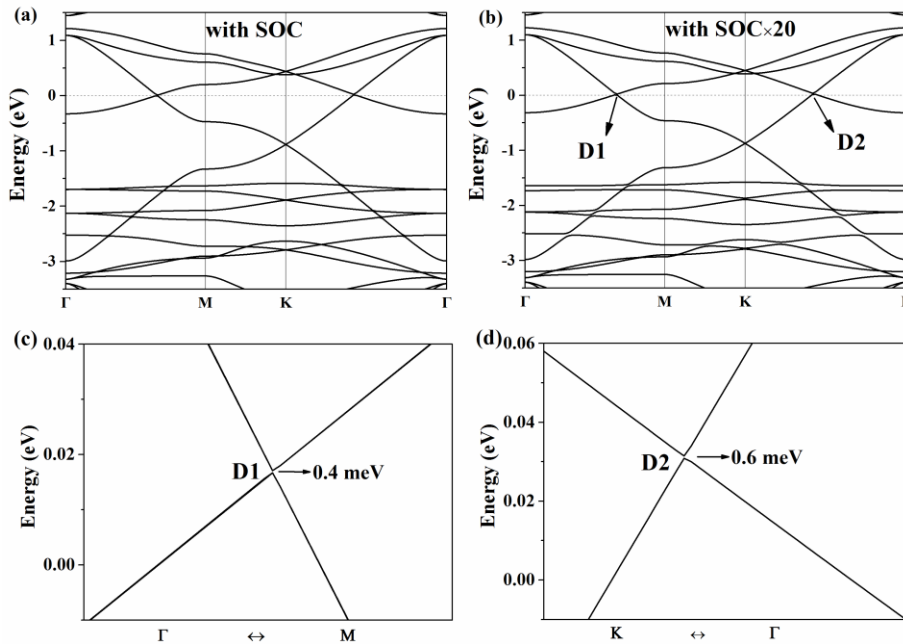


Fig. S4 (a) Band structure for C_9N_4 calculated with SOC and (b) artificially increased SOC strength (20 times larger) respectively. (c)-(d) Enlarged band structures around touch points D1 and D2 indicated in (b). The Fermi level is set as zero.

- Details about molecular properties of C_9N_4 .

To better understand the formation of the intrinsic nodal ring in our 2D covalent network system, we carried out quantum chemistry calculation about the molecular properties of the organic building unit ($C_9N_4H_6$) using Gaussian package. Based on DFT calculation results, we know that both the Dirac and Kagome bands are formed solely by the p_z orbitals of hybridized C and N atoms, thus, it is reasonable to only focus on the π molecular orbitals (MOs) formed by conjugated p_z orbitals. Each atom contributes one p_z orbital leading to a total of 13 π MOs. By analyzing the local environment of each atom, the total number of π electrons is counted to be 14 (two for the central N and one for the other atoms). Therefore there are 7 MOs filled, which is further confirmed by our calculation results from Gaussian package.

As shown in Fig. S3(a), we plotted the three most related MOs of $C_9N_4H_6$, i.e., one highest occupied MO (HOMO) and two lowest unoccupied MOs (LUMOs). It is important to note that the first LUMO shows exact shape as that of the partial charge of the Dirac bands, and the first HOMO and the second LUMO show similar feature as that of the Kagome bands (nearly zero contribution from the central N atom). Further, we calculate the MOs of $(C_9N_4H_4)_2$, shown in Fig. S1(b), which possesses exact number of π electrons as in our 2D covalent system, which in principle will yield instructive information about the electron filling in forming the C_9N_4 crystalline. It can be clearly seen that the left and right MOs of the $C_9N_4H_6$ form new bonding and anti-bonding MOs in $(C_9N_4H_4)_2$. The first two new LUMOs are almost identical to the

partial charge plotted for the upper and lower Dirac bands, and the two HOMOs and the third and fourth LUMO show similar feature as that of Kagome bands. In forming the periodic 2D covalent crystalline, these MOs will form the Dirac and Kagome bands respectively.

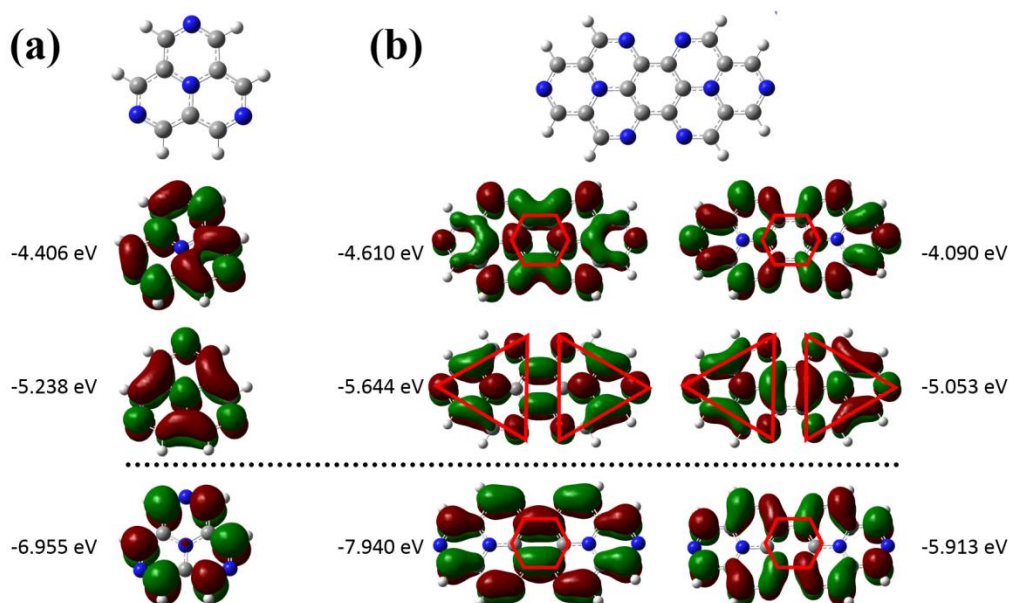


Fig. S5 Molecular information of the organic fundamental unit. (a) MO diagram of the single $C_9N_4H_6$. (b) MO diagram of the $(C_9N_4H_4)_2$ showing the bonding and anti-bonding feature of the MOs from $C_9N_4H_6$. The red hexagon and triangle indicate MOs feature from Dirac and Kagome bands respectively.

Moreover, the MOs that form the Dirac bands are fully unoccupied, and the MOs that construct the Kagome bands are partially filled (two HOMOs), which explains the band filling results calculated from DFT, i.e., nearly unfilled Dirac band and 2/3 filled Kagome bands. On the other hand, the energy difference between the MOs that form Dirac bands is much smaller than that of the MOs forming Kagome bands which help explaining the crossover between the two sets of bands that giving rise to the Nodal ring. We note that our molecular calculation could not exactly reproduce the MOs of the Kagome bands because of the lack of periodic boundary condition as well as the crystal symmetry in our molecular calculation. Due to the same reason, the

interaction between MOs that form Dirac and Kagome bands will be slightly changed from our calculation.

- Total energy comparison and band structure for AB-stacking and AA-stacking

C_9N_4

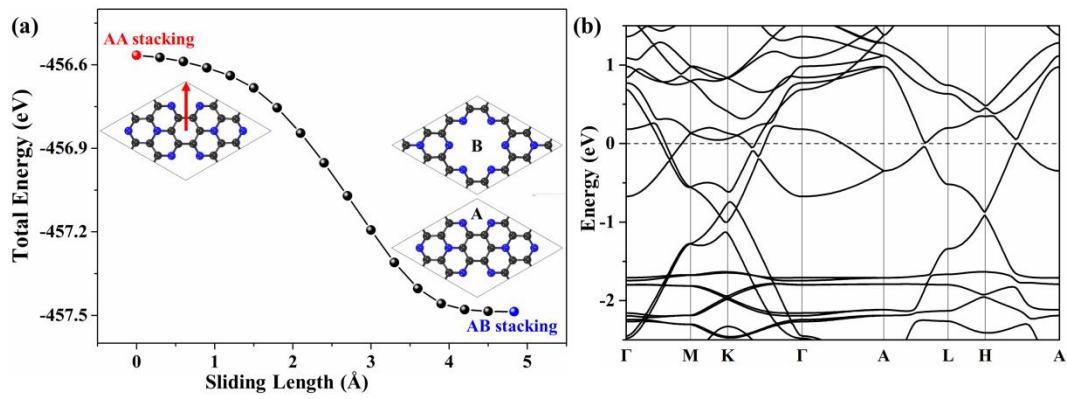


Fig. S6 (a) Total energy for bulk C_9N_4 with different stacking configurations. The red and blue dots present the AA and AB type stacking, respectively. Other structures between red and blue dots are generated by shifting the top A-layer in AA-stacking along the red arrow until reaching the position of AB-stacking. The right inset in (a) shows the top A-layer and bottom B-layer in AB-stacking form. (b) The band structure for optimized AB- C_9N_4 .

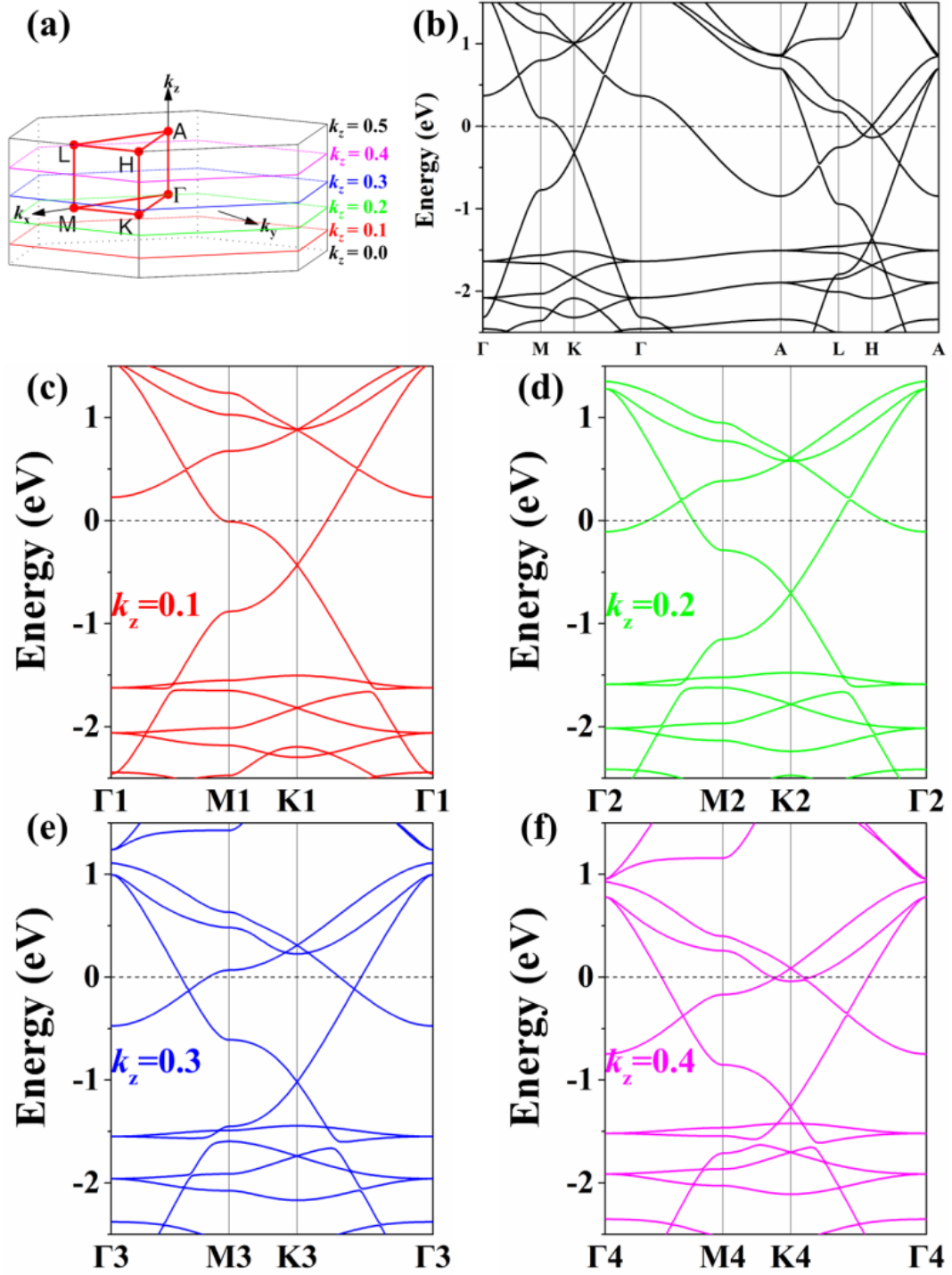


Fig. S7 (a) BZ for AA-stacking C_9N_4 . (b) Band structure for AA-stacking C_9N_4 along high-symmetry paths in the BZ. (c)-(f) Band structure for AA-stacking C_9N_4 on $k_z = 0.1, 0.2, 0.3,$ and 0.4 plane.

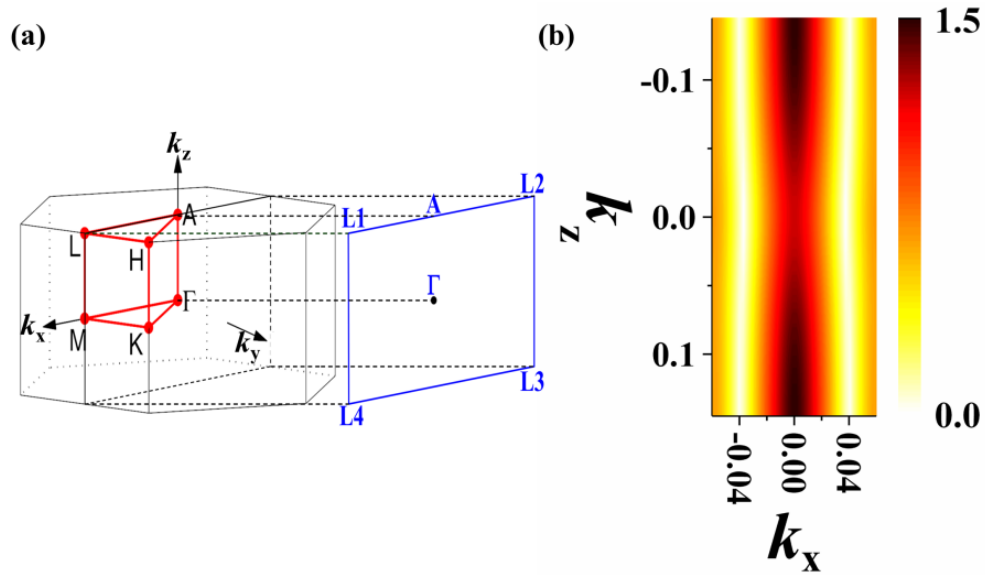


Fig. S8 (a) BZ for AA-stacking C_9N_4 , the blue rectangle represents the $k_y=0$ plane. (b) Projected band structure on $k_y=0$ plane, where the color bar indicates the energy difference between conduction and valence bands at each k point, the two nodal-lines is shown in color white.

- Details related to the C_9N_4 Stability.

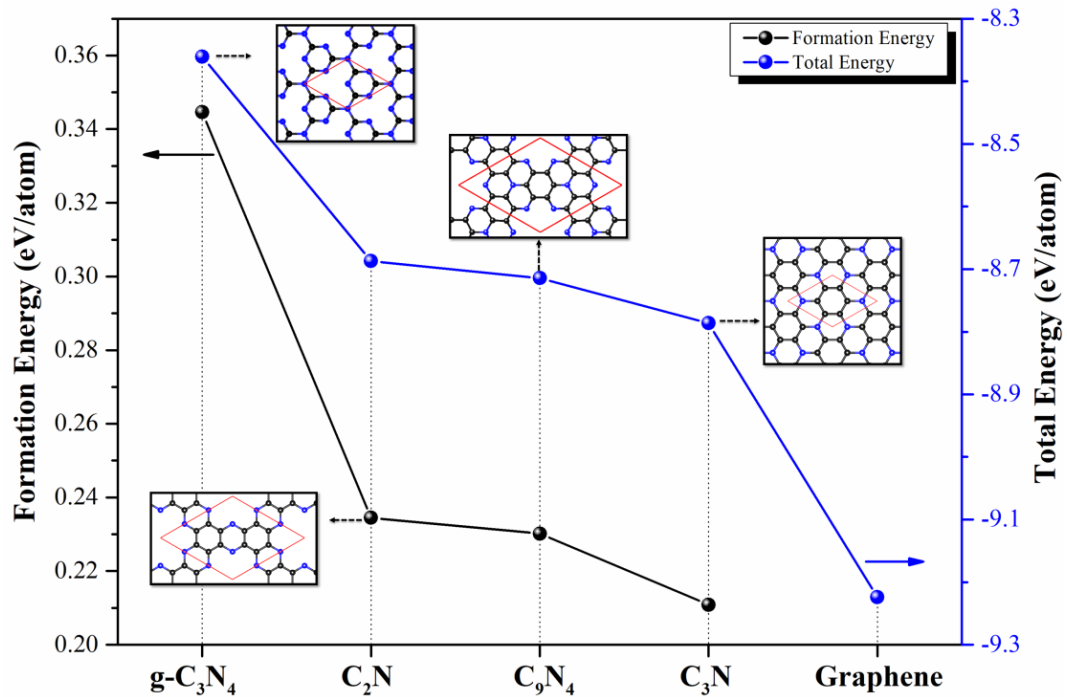


Fig. S9 Calculated total energy (eV/atom) of monolayer C_9N_4 compared with 2D graphene, C_3N , C_2N , and $g-C_3N_4$.

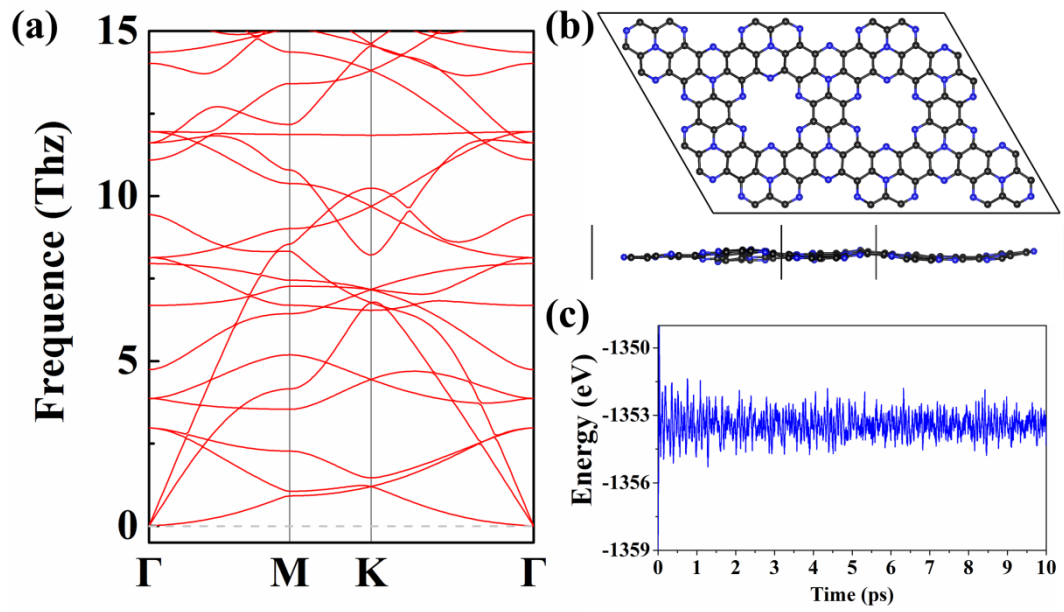


Fig. S10 (a) Phonon spectra for C₉N₄ along high-symmetry paths in the BZ. (b) Top and (c) Side views of final snapshot of monolayer C₉N₄ atomic structure after AMID simulations for 10 ps. The time step is 1 fs.